Radiotherapy and Oncology 174 (2022) 149–157

Contents lists available at ScienceDirect

Radiotherapy and Oncology

journal homepage: www.thegreenjournal.com

Original Article

First experimental demonstration of VMAT combined with MLC tracking for single and multi fraction lung SBRT on an MR-linac

Prescilla Uijtewaal [a,*], Pim T.S. Borman [a], Peter L. Woodhead [a,b], Charis Kontaxis [a], Sara L. Hackett [a], Joost Verhoeff [a], Bas W. Raaymakers [a], Martin F. Fast [a]

[a] Department of Radiotherapy, University Medical Center Utrecht, Heidelberglaan 100, Utrecht, 3584 CX Utrecht, the Netherlands; [b] Elekta AB, Stockholm, Sweden

ARTICLE INFO

Article history:
Received 24 December 2021
Received in revised form 8 June 2022
Accepted 3 July 2022
Available online 9 July 2022

Keywords:
Lung cancer
MLC tracking
VMAT
MR-linac
Prediction

ABSTRACT

Background and purpose: VMAT is not currently available on MR-linacs but could maximize plan conformality. To mitigate respiration without compromising delivery efficiency, MRI-guided MLC tumour tracking was recently developed for the 1.5 T Unity MR-linac (Elekta AB, Stockholm, Sweden) in combination with IMRT. Here, we provide a first experimental demonstration of VMAT + MLC tracking for several lung SBRT indications.

Materials and methods: We created central patient and phantom VMAT plans (8×7.5 Gy, 2 arcs) and we created peripheral phantom plans (3×18 & 1×34 Gy, 4 arcs). A motion phantom mimicked subject-recorded respiratory motion ($\overline{A}$=11 mm, $\overline{f}$=0.33 Hz, $\overline{drift}$=0.3 mm/min). This was monitored using 2D-cine MRI at 4 Hz to continuously realign the beam with the target. VMAT + MLC tracking performance was evaluated using 2D film dosimetry and a novel motion-encoded and time-resolved pseudo-3D dosimetry approach.

Results: We found an MLC leaf and jaw end-to-end latency of 328.05(±3.78) ms and 317.33(±4.64) ms, which was mitigated by a predictor. The VMAT plans required maximum MLC speeds of 12.1 cm/s and MLC tracking superimposed an additional 1.48 cm/s. A local 2%/1 mm gamma analysis with a static measurement as reference, revealed pass-rates of 28–46% without MLC tracking and 88–100% with MLC tracking for the 2D film analysis. Similarly, the pseudo-3D gamma passing-rates increased from 22–77% to 92–100%. The dose area histograms showed that MLC tracking increased the GTV $D_{98\%}$ by 5–20% and the PTV $D_{95\%}$ by 7–24%, giving similar target coverage as their respective static reference.

Conclusion: MRI-guided VMAT + MLC tracking is technically feasible on the MR-linac and results in highly conformal dose distribution.

A viable alternative for surgery to treat early stage non-small-cell lung cancer is stereotactic body radiation therapy (SBRT) [1,2]. The dose distributions need to be highly conformal around the target to ensure coverage, while sparing adjacent organs at risk (OARs) [3]. Although Intensity Modulated Radiation Therapy (IMRT) produces conformal dose distributions, Volumetric Modulated Arc Therapy (VMAT) can in some cases spare even more tissue with equal target coverage [4]. On C-arm linacs, VMAT typically reduces delivery times when combined with high-dose rate flattening-filter free beams [5]. These benefits make VMAT a standard delivery technique for lung SBRT. However, both the 0.35 T MRIdian (ViewRay Inc., Oakwood, USA) and the 1.5 T Unity MR-linac (Elekta AB, Stockholm, SWE) exclusively support fixed-beam IMRT delivery in clinical mode. To show that the MR-linac is capable of delivering VMAT plans, a recent study explored VMAT deliveries on Unity for prostate SBRT [6].

The dose conformity of IMRT and VMAT increases the need for respiratory motion management. Current options to achieve this include: internal target volume (ITV; Unity) [7], or gating (MRIdian) [8]. The ITV provides GTV coverage by covering the full tumour motion, which for lung SBRT is typically 1–3 cm in cranial-caudal (CC) direction [9–11]. ITVs are relatively large and might overlap with OARs near central tumours, increasing toxicity risks [12,2]. Contrastingly, gating irradiates the tumour only during parts of the breathing cycle, requiring smaller treatment margins [13,8]. However, gating also drastically extends beam-on times with only 50–60% duty cycle [14,15], which is especially concerning for single fraction treatments [14]. Gating efficiency can be improved by breath-hold techniques, but this requires patient compliance [16]. An alternative is multi-leaf collimator (MLC) tracking, which realigns the treatment beam with the most recently observed (or predicted) tumour position [17,18]. MLC

* Corresponding author at: Heidelberglaan 100, 3584 CX Utrecht, the Netherlands.
E-mail address: p.uijtewaal-2@umcutrecht.nl (P. Uijtewaal).

https://doi.org/10.1016/j.radonc.2022.07.004
0167-8140/

tracking uses similar treatment margins as gating, while maintaining a 100% duty cycle. MLC tracking is well established in the context of C-arm linacs [19–21]. Previous experiments demonstrated MRI-guided MLC tracking on the MR-linac either for artificial [22,17] and subject-recorded [23] respiratory CC-motion for a single gantry angle with a conformal treatment field, or for IMRT treatments with artificial CC-motion [24]. To our knowledge, MLC tracking has not been demonstrated before on the MR-linac in combination with VMAT.

Combining VMAT with MRI-guided MLC tracking is complex, because the leaf and jaw motion of both dynamic modes is superimposed. Previous studies investigated the technical feasibility of VMAT + MLC tracking for C-arm linacs [25–27] or demonstrated its feasibility in clinical trials [28]. Besides the ability to directly

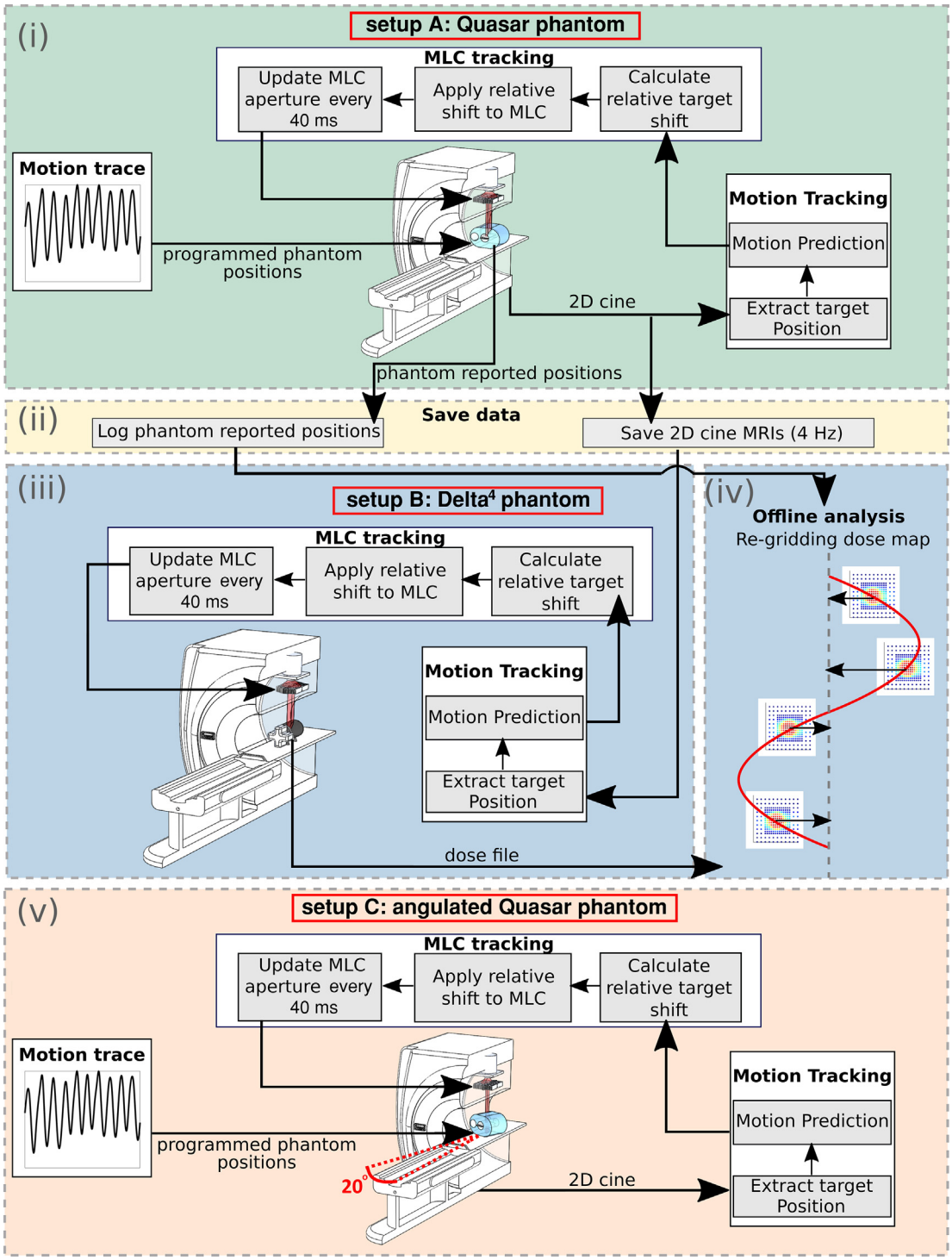

Fig. 1. Experimental setup for VMAT + MLC tracking on the MR-linac. Setup A (i) uses the Quasar phantom (CC-only motion). (ii) The phantom reported positions and MRIs from setup A are saved (ii) and used in setup B (iii) the Delta^4 phantom with a virtual HexaMotion platform (iv). (v) Setup C uses the angulated Quasar phantom (CC and LR motion).

monitor the target motion with MRI, the unique engineering setup of the MR-linac differs from any C-arm linac. Differences include: very fast gantry rotation, very fast MLC speed (>12.1 cm/s), fixed collimator angle (270°), low dose rate (425 MU/min), and the ability to continuously rotate; which necessitate a detailed study of VMAT + MLC tracking on the MR-linac.

In this study, we provide a first experimental demonstration of VMAT combined with MLC tracking for a range of lung SBRT fractionation schemes. The VMAT + MLC tracking performance both for phantom and patient treatment plans was evaluated using 2D film dosimetry setups and a novel motion-encoded and time-resolved pseudo-3D dosimetry approach.

Materials and methods

All experiments were performed on an Elekta Unity MR-linac, featuring a 1.5 T MR scanner and a 7 MV linac. The radiation beam is shaped in CC direction using a 160-leaf MLC consisting of 7.125 mm wide leaves with fixed collimator angle, while dynamic jaws limit the radiation field perpendicular to the leaf travel direction.

In our experimental setup we used the Quasar MRI^{4D} phantom (Modus Medical Devices Inc., London ON) and the Delta^4 Phantom+ (ScandiDos, Sweden) for dosimetry.

VMAT + MLC tracking

This work used interfaces developed for research to combine VMAT [6] with MRI-guided MLC tracking [24]. The interfaces contain an optimized proportional–integral–derivative (PID) control loop of the MLC motors to better support dynamic deliveries. To apply MLC tracking, we updated the leaf and jaw positions every 40 ms according to the predicted tumour position [24], thus correcting for translational target motion.

Imaging

The phantom motion was continuously monitored using sagittal 2D cine-MR [24]. Images were acquired using a T1-weighted gradient-echo sequence at 4 Hz, with a 2.5×2.5 mm^2 voxel size and 350×350 mm^2 field of view. Target positions were estimated from the images using cross-correlation based template matching [29].

Latency & Prediction

End-to-end latency, defined as the time lag between a physical motion event and the MLC response [30,24,22], causes dosimetric errors during MRI-guided MLC tracking. To estimate the average end-to-end latency, the Quasar MRI^{4D} phantom with circular 10 mm target was programmed with sinusoidal CC motion (A = 10 mm, T = 4 s). A squared 5×5 cm^2 aperture tracked the target based on MR derived positions. An integrated electronic portal imaging device panel detected the target and MLC-aperture positions. Based on the phase difference between the two sets of positions, the end-to-end latency was estimated [30,19]. We derived the end-to-end leaf ($\tau_{leaf}^{measured}$) and jaw ($\tau_{jaw}^{measured}$) latency independently. Because the phantom has only one translational motion axis and it does not fit in the bore transversely, $\tau_{jaw}^{measured}$ was estimated by software-wise mapping the phantom's CC motion to left-right (LR) motion such that the tracking software assumed pure LR motion and moved the jaws in LR direction to track the motion.

A linear ridge regression predictor mitigated the end-to-end latency by using past tumour positions to predict the next position [24]. The small difference between $\tau_{leaf}^{measured}$ and $\tau_{jaw}^{measured}$ was not accounted for in the prediction.

Dosimetry setup

The dosimetric benefit of VMAT + MLC tracking was assessed by comparing static deliveries to deliveries with respiratory motion in three different experimental setups (Fig. 1):

- **Setup A:**
  Setup A (Fig. 1i) used the Quasar phantom with gafchromic EBT-3 or EBT-XD film. This setup was previously used for IMRT + MLC tracking [24]. We programmed the Quasar with a

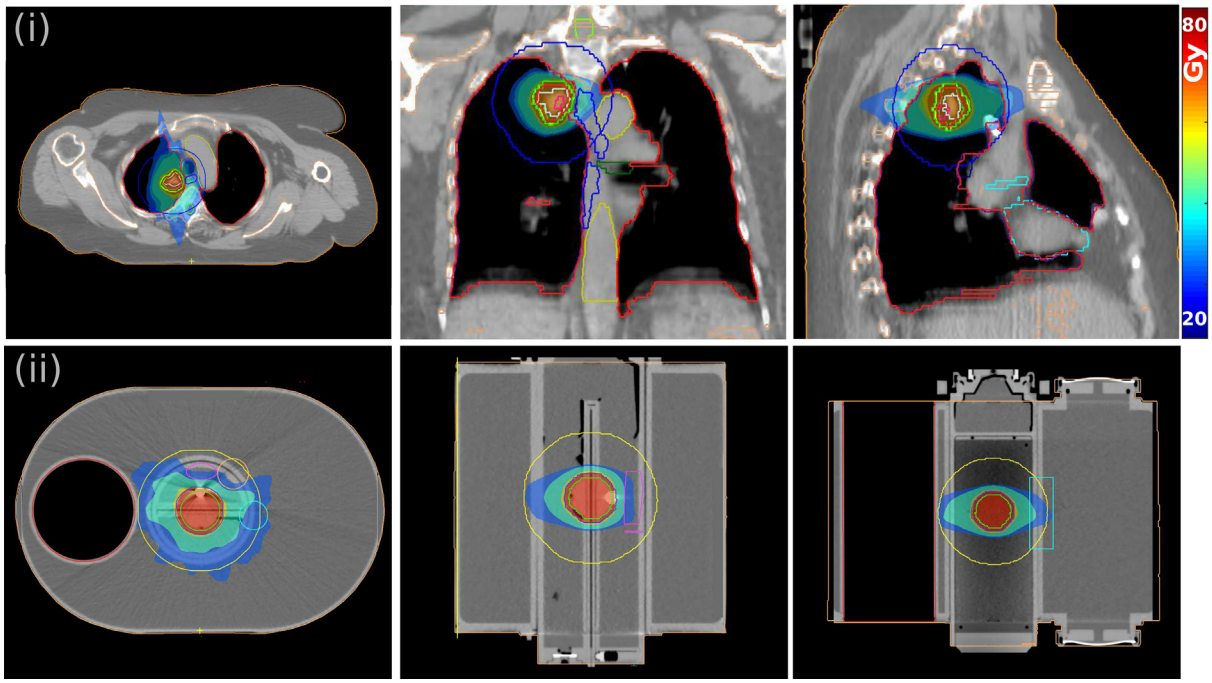

Fig. 2. Example central lung SBRT VMAT plans for (i) patient 1 and (ii) the Quasar phantom.

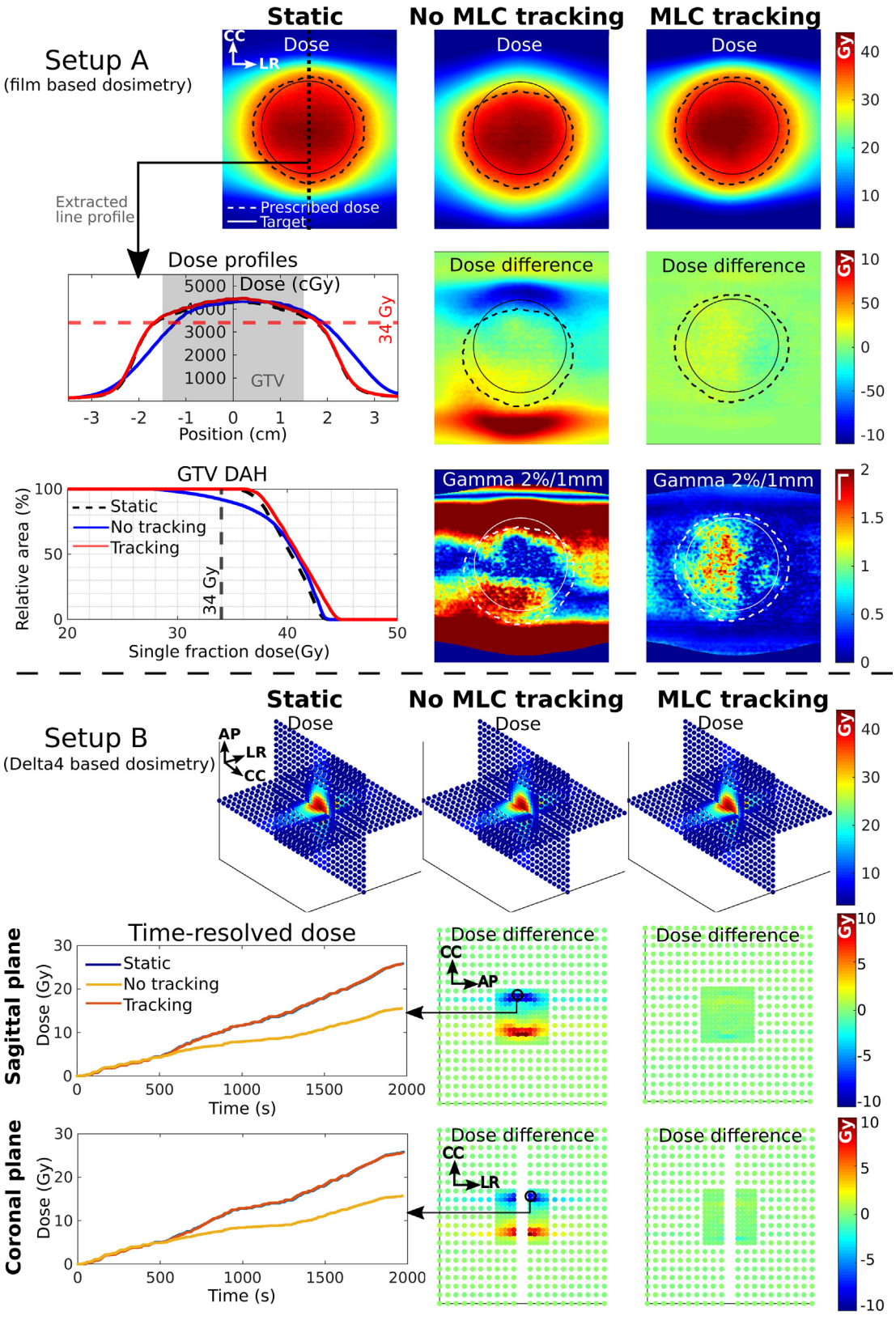

Fig. 3. Dosimetric results of setup A&B for the 1×34 Gy delivery with CC motion. Dose difference maps compare the cases with and without MLC tracking to a static delivery. The solid and dashed circles (A) indicate the GTV and the prescription iso-dose line. The GTV DAH reveals the relative target coverage. The grey area in the dose profiles indicate the GTV position. The time-resolved dose figures indicate how much dose was delivered to a single diode over time. Note that the dose lines of the static and MLC tracking case are superimposed.

subject-recorded motion trace containing respiratory CC motion ($\overline{A}$=11 mm, $\overline{f}$=0.33 Hz, $\overline{drift}$=0.3 mm/min). The phantom contained a film insert with 3 cm spherical target (GTV) that was positioned centrally or peripherally (10 cm off-center) in a water-filled body oval. Recorded 2D cine MRIs used for MLC tracking and the current positions simultaneously reported by the phantom (phantom reported positions) were saved for later use in Setup B.

- **Setup B:**
  Setup B (Fig. 1iii) used the Delta^4 phantom [31] with research software enabling VMAT support and time-resolved data export/input. It was longitudinally positioned in the bore either centrally or with a lateral offset, depending on the lateral position of the tumour. Two orthogonal planes (coronal and sagittal) filled with diodes measure dose every 25 ms. Diodes in the central 6×6 cm^2 are spaced 5 mm apart, with 10 mm spacing elsewhere. The phantom cannot move and its electronics disallow real-time MR-imaging. Therefore, we used the Quasar in setup A to pre-record phantom motion using 2D-cine MRI at 4 Hz and simultaneously logged the phantom reported (ground-truth) positions on the same workstation. The positions were streamed to the tracking software as if they were acquired online.
  Because the Delta^4 is immovable, the measured dose during MLC tracking is spread out relative to a static delivery. To retrospectively evaluate the notional VMAT + MLC tracking performance, we created a *virtual* HexaMotion platform. We virtually moved the phantom with the target by shifting the measured incremental dose (every 25 ms) by the same amount but in opposite direction as the target had moved w.r.t the isocenter. Dose shifts were carried out by re-gridding the data using cubic spline interpolation.
- **Setup C:**
  Setup C (Fig. 1v) was derived from Setup A, but with the phantom rotated by 20° around the anteroposterior axis to decompose the phantom motion into CC motion ($\overline{A}$=10 mm) and LR motion ($\overline{A}$=4 mm). This enables MLC tracking in both CC and LR direction.

Treatment planning

For our experiments, we used four patient lung SBRT plans with a central lung tumour and eight phantom plans for both central and peripheral indications. Planning CTs were acquired on the Brilliance Big Bore CT scanner (Philips Medical Systems, Best, The Netherlands). Patients underwent 4D-CT imaging from which an averaged 3D-CT image was reconstructed, while the Quasar phantom was imaged using 3D-CT. For each patient an ITV was delineated by a radiation oncologist and an isotropic 3 mm ITV-to-PTV margin was used following the institutional practice. In the phantom, the target was delineated as GTV and an isotropic 3 mm GTV-to-PTV margin was used. Additionally, an oesophagus, bronchus and aorta were delineated as OAR for central phantom plans. No OARs were delineated for the peripheral phantom plans. For each patient case, an 8×7.5 Gy VMAT plan was created by adapting the patient's clinically approved lung SBRT IMRT plan to a VMAT plan (Fig. 2) in research Monaco 5.51.10 (Elekta AB, Stockholm, Sweden). For the phantom we created four VMAT plans for both experimental setup A and C by adapting the clinical lung SBRT template: two central 8×7.5 Gy two-arc plans with and without OAR, and two peripheral 3×18 Gy and 1×34 Gy four-arc plans. Setup B used the same plans as setup A, but calculated for the Delta^4. Following our clinical template, in all plans the maximum dose in the GTV was limited to 145% of the prescription dose

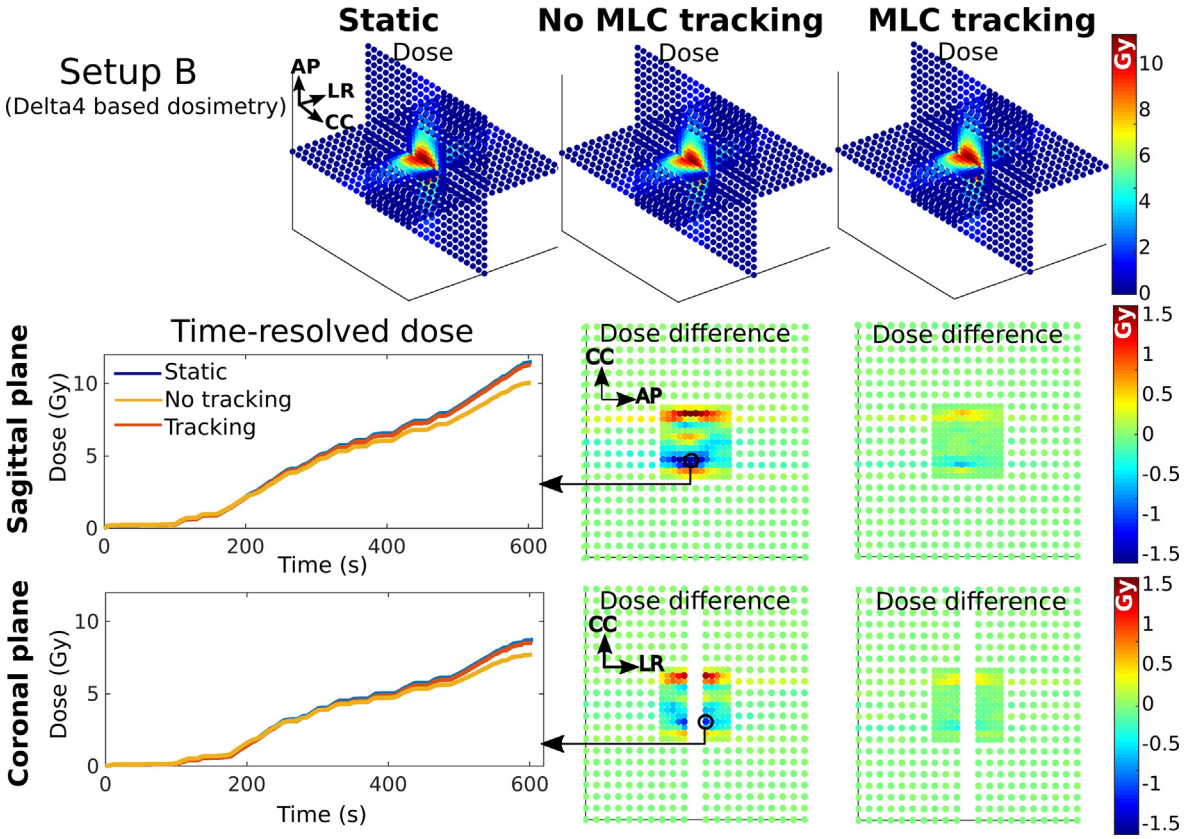

Fig. 4. Dosimetric results of patient 1 in setup B. Dose difference maps compare the cases with and without MLC tracking to a static delivery.

(PD). Retrospective MU scaling was applied for all plans to provide a PTV coverage of 95% of the PD. Gantry angles 5–25° were excluded from the arcs, to avoid irradiating the cryostat pipe. Plans were calculated with 3 mm grid size and 8% Monte Carlo uncertainty per segment, following our current clinical practice.

Dosimetric evaluation

The irradiated EBT-3 and EBT-XD films were scanned and digitized with an Epson Expression 10000XL flatbed scanner (Seiko Epson Corp, Nagano, Japan). To analyse the films we used in-house developed software. The films were semi-automatically registered with a point matching algorithm, based on three indents created by the phantom's film cassette. A 2%/1 mm local gamma-analysis evaluated the correspondence between static and MLC tracking deliveries for film and Delta[4] measurements. Only dose values with >10% PD were analysed, to reduce calibration induced uncertainties. For the film dosimetry, the GTV-coverage was quantified using dose area histograms (DAHs).

Plan deliverability calculation

We determined if the leaf and jaw motion of the VMAT delivery might be affected by the superimposed MLC tracking motion. The leaf/jaw speeds necessary for VMAT were based on the static delivery log files. Only segment shaping leaves were included, to avoid underestimation of the speeds due to static leaves outside the segment shape. Additional leaf/jaw speeds necessary to track CC motion in setup A&B and CC + LR motion in setup C were based on the motion trajectory. The required leaf/jaw speeds were expressed as the near-maximum (95th percentile) and the maximum (99th percentile) speed.

Results

For $\tau_{leaf}^{measured}$ and $\tau_{jaw}^{measured}$ we found an end-to-end latency of 328.05(±3.78) ms and 317.33(±4.64) ms. The predictor reduced these to 0.04(±3.17) ms and 34.86(±4.58) ms. The patient plans were delivered in 10.3–12.3 min and the phantom plans were delivered in 7.2–7.5 min (8×7.5 Gy), 18.1–19.3 min (3×18 Gy), and 30.0–32.5 min (1×34 Gy). These times were not affected by MLC tracking. The films were registered with an average error of 0.37(±0.25) mm. The plans required near-maximum leaf and jaw speeds of 0.4–2.2 cm/s and 0.2–0.6 cm/s, and maximum speeds of 1.5–12.1 cm/s and 0.9–3.2 cm/s. MLC tracking required additional near-maximum leaf and jaw speeds of 1.26 cm/s and 0.43 cm/s and maximum speeds of 1.48 cm/s and 0.51 cm/s.

Fig. 3 shows an overview of the dosimetric results of setup A&B for the 1×34 Gy delivery. The dose difference maps emphasize that without MLC tracking the delivered dose differs from a static delivery, while the MLC tracking case is very similar. The delineated target in the dose maps (Fig. 3A) shows that without MLC tracking, parts of the GTV drift outside the prescription iso-dose line, indicating underdosage of the cranial GTV edge. This is supported by

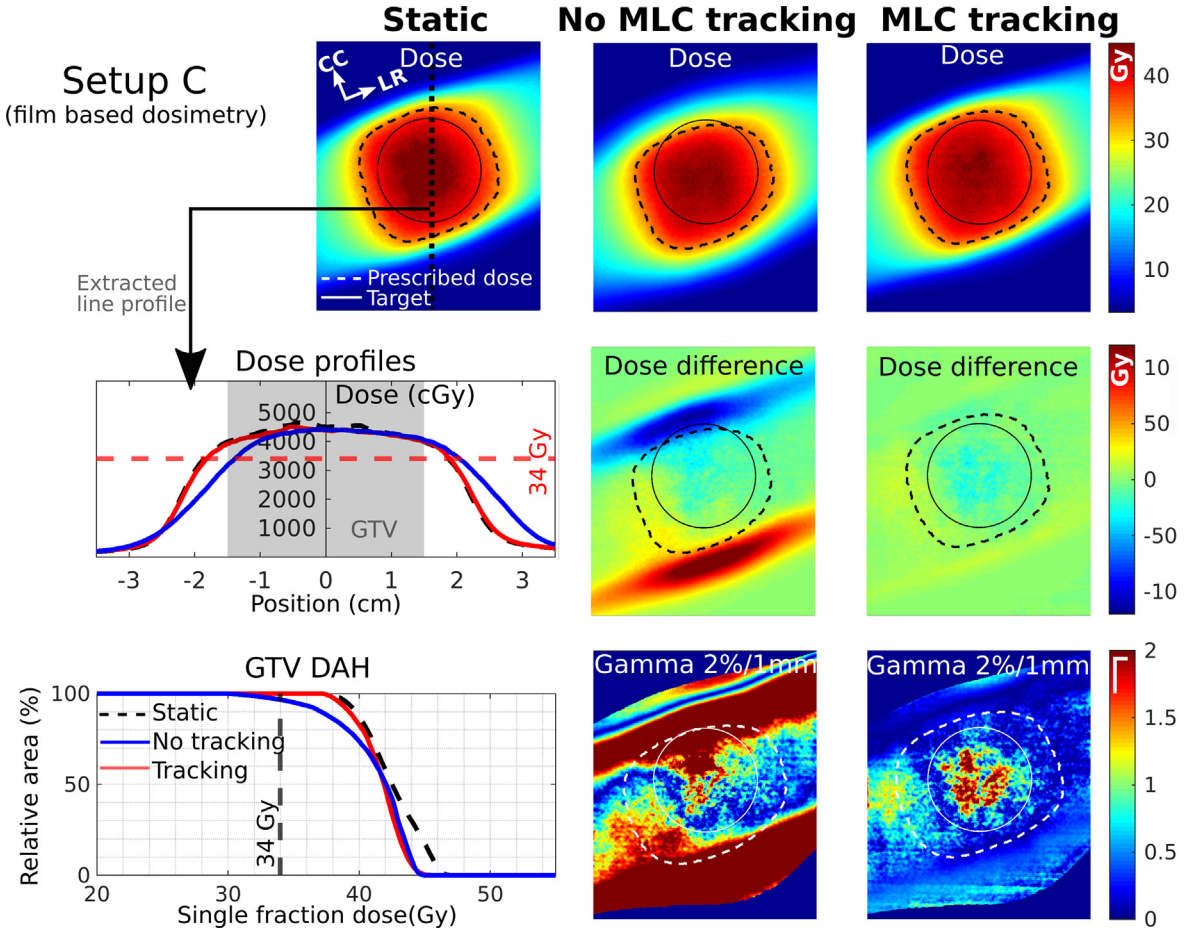

Fig. 5. Dosimetric results of setup C for the 1×34 Gy delivery with CC and LR motion. Dose difference maps compare the cases with and without MLC tracking to a static delivery. The solid and dashed circles indicate the GTV and the prescription iso-dose line. The GTV DAH reveals the relative target coverage. The grey area in the dose profiles indicates the GTV position.

the DAH and the dose profiles. The time-resolved dose graphs (Fig. 3B) show the dose of a single diode. Initially, it receives the same dose in all three cases. After about 500 s the no MLC tracking case starts receiving less dose, which coincides with increased drift in the motion trace. Fig. 4 shows similar results for patient 1, where the dose with MLC tracking agrees well with the static dose, while without MLC tracking the dose differs.

Fig. 5 shows the results for a 1×34 Gy delivery of setup C. Here, MLC tracking and static dose maps also agree well, while without MLC tracking this agreement markedly deteriorates. The delineated target in the dose maps, the DAH and the line profiles show that MLC tracking effectively avoids underdosage of the GTV.

Table 1 summarizes the gamma pass-rates and DAH metrics in the different setups. MLC tracking yields gamma pass-rates of 88–100% for film measurements in setup A&C and 92–100% for the Delta^4 in setup B. The peripheral plans have lower pass-rates without MLC tracking (22–38%) than the central deliveries (34–77%). These deliveries are longer and accumulate more drift. The gamma pass-rates for the phantom plans are similar to the pass-rates of the patient plans. The DAH results in Table 1 show similar GTV and PTV coverage for the static and MLC tracking cases, with dose differences within the GTV ranging between 0–15 cGy (8×7.5 Gy), 5–102 cGy (3x18 Gy), 26–176 cGy (1×34 Gy) for the $D_{98\%}$, $D_{50\%}$, and $D_{2\%}$ GTV dose. Without MLC tracking, the GTV $D_{98\%}$ reduces by 25–55 cGy (8×7.5 Gy), 254–378 cGy (3×18 Gy), and 575–645 cGy (1×34 Gy), resulting for the peripheral cases in severe underdosage. Both in setup A&C, the PTV $D_{95\%}$ benefits from MLC tracking. Again the peripheral cases benefit most, as MLC tracking is needed there to achieve sufficient coverage. The GTV $D_{50\%}$ and $D_{2\%}$ were similar to the static case.

Discussion

In this study, we demonstrate the first experimental setup that combines VMAT with MRI-guided MLC tracking on an MR-linac. For a range of lung SBRT fractionation schemes, we demonstrate with our novel phantom setups that MLC tracking excellently compensates for respiratory motion during VMAT resulting in similar dose distributions and target coverage as during a static delivery.

The end-to-end leaf latency (328.05±3.78 ms) was in line with previously reported values on Unity [24,22]. We found $\tau_{jaw}^{measured}$ to be very similar to $\tau_{leaf}^{measured}$. We initially expected more latency for the heavier jaws, but because their motor controller compensates for their weight, the latency is similar. The predictor effectively mitigated the end-to-end latency. Because $\tau_{jaw}^{measured}$ is lower than $\tau_{leaf}^{measured}$, we slightly over predicted for $\tau_{jaw}^{measured}$, leaving a negligible residual end-to-end latency of 34.86(±4.58) ms. To deliver our VMAT plans, we required maximum MLC speeds of 12.1 cm/s. MLC tracking required additional speeds of maximally 1.48 cm/s. With these maximum speeds as determined, the MLC was still able to follow the combined VMAT and MLC tracking motion.

We introduced three experimental setups to show the dosimetric benefits of MLC tracking during VMAT for lung SBRT. The results prove that VMAT benefits from MLC tracking, providing dose distributions very similar to the corresponding static delivery with local gamma pass-rates >88%. These values are in line with previously reported pass-rates for IMRT + MLC tracking [24]. For our motion trajectory, MLC tracking mainly benefits the coverage of the target periphery. Lung tumours may experience a baseline drift of up to 0.9 mm/min [32], meaning that they can easily drift outside the

Table 1
DAH and gamma pass-rates that compare plans with and without MLC tracking to a static delivery for the different prescriptions and setups. Note that DAHs were not available for setup B and for the patient plans.

	Setup A					Setup B	Setup C				
	Gamma pass-rate (2D)	DAH GTV			DAH PTV	Gamma pass-rate (pseudo-3D)	Gamma pass-rate (2D)	DAH GTV			DAH PTV
	(2%/1 mm)	$D_{98\%}$ (cGy)	$D_{50\%}$ (cGy)	$D_{2\%}$ (cGy)	$D_{95\%}$ (cGy)	(2%/1 mm)	(2%/1 mm)	$D_{98\%}$ (cGy)	$D_{50\%}$ (cGy)	$D_{2\%}$ (cGy)	$D_{95\%}$ (cGy)
Central delivery W/o OAR (8×7.5 Gy)											
Static	-	928	1038	1120	835	-	-	887	1000	1084	808
No MLC tracking	34	873	1007	1078	771	77	46	832	963	1045	743
MLC tracking	100	921	1032	1114	829	100	100	887	999	1092	803
W/ OAR (8×7.5 Gy)											
Static	-	805	844	882	759	-	-	830	928	992	765
No MLC tracking	44	780	839	882	725	69	28	780	892	935	705
MLC tracking	93	816	855	897	776	93	97	844	929	978	777
Patient 1 (8×7.5 Gy)											
No MLC tracking	-	-	-	-	-	56	-	-	-	-	-
MLC tracking	-	-	-	-	-	96	-	-	-	-	-
Patient 2 (8×7.5 Gy)											
No MLC tracking	-	-	-	-	-	49	-	-	-	-	-
MLC tracking	-	-	-	-	-	92	-	-	-	-	-
Patient 3 (8×7.5 Gy)											
No MLC tracking	-	-	-	-	-	43	-	-	-	-	-
MLC tracking	-	-	-	-	-	97	-	-	-	-	-
Patient 4 (8×7.5 Gy)											
No MLC tracking	-	-	-	-	-	56	-	-	-	-	-
MLC tracking	-	-	-	-	-	96	-	-	-	-	-
Peripheral delivery (3×18 Gy)											
Static	-	1959	2206	2404	1812	-	-	1871	2110	2334	1761
No MLC tracking	33	1581	2130	2317	1395	38	33	1617	2057	2238	1461
MLC tracking	88	1930	2144	2302	1785	99	92	1908	2146	2329	1784
(1×34 Gy)											
Static	-	3543	3960	4239	3292	-	-	3845	4252	4626	3614
No MLC tracking	28	2898	4006	4359	2539	22	30	3270	4206	4444	2942
MLC tracking	93	3610	4025	4362	3333	100	92	3794	4190	4450	3588

3 mm GTV-to-PTV margin during longer treatments. In our experiments, the central phantom deliveries were relatively short deliveries of only 7 min resulting in little accumulated drift. This means that during the central deliveries the target did not drift out of the PTV margin, which explains that also without MLC tracking both the GTV and PTV coverage were hardly affected. This is also reflected in the relatively high Delta^4 gamma-pass rate, where the motion was too subtle considering the relatively coarse diode spacing. For the higher dose peripheral deliveries, combining VMAT with MLC tracking is crucial to restore target coverage, as these deliveries are long due to the relatively low dose rate of Unity (425 MU/min).

A limitation of our dosimetric evaluation is that experimental setups A&C only evaluate dose in a single coronal plane intersecting the center of the target, while neglecting the rest of the target. The Delta^4 in setup B expands this evaluation from 2D to pseudo-3D by adding a sagittal plane to the evaluation. The results demonstrated that the effect of MLC tracking is identical in both planes, confirming the benefits of MLC tracking for VMAT. The time-resolved and motion included aspects of setup B, can also be expanded to applications outside this study.

Other than restoring target coverage, MLC tracking also reduced hot spots during VMAT outside the GTV as visible in the dose difference maps. Especially in the 1×34 Gy deliveries without MLC tracking, there is up to 15 Gy extra dose outside the GTV compared to the static case. These undesired high dose areas could damage surrounding tissue [2,12]. This is also important for central tumours, for which intensified hypofractionation is currently often not recommended because of toxicity risks [33]. The high precision of VMAT + MLC tracking could increase the feasibility of single fraction deliveries for more patients, while also increasing patient comfort with the possibility of free-breathing during treatment and no extended beam-on times (100% duty cycle). This is especially true for patients with substantial tumour motion.

Neither MLC tracking nor VMAT are in the current clinical MR-linac release. Although we demonstrated the technical feasibility of VMAT + MLC tracking on the MR-linac, further work is needed to develop an integrated clinical workflow. The clinical treatment planning (TPS) system needs to fully support VMAT on Unity, especially for daily plan adaptation. Our research TPS occasionally creates segments with very low dose rates, limiting the deliverability of a plan. It also creates closed segments where leaves have to fully close and open in two consecutive segments, which is difficult to track because of the required additional leaf speed. Additionally, the imaging and motion estimation workflow needs to be tailored to patients [34]. The current sequence only images a 2D sagittal plane, as it was developed for the Quasar. Monitoring through-plane motion is crucial in real patients to avoid losing the target when it moves out of plane. To avoid increasing the system latency with relatively slow 3D sequences, interleaved orthogonal 2D-cine MRIs can be used to track 3D tumour motion [35,36] combined with a prediction filter to mitigate latency [36].

Conclusions

We provided a first experimental demonstration of the technical feasibility of VMAT + MLC tracking on an MR-linac for several lung SBRT indications. MLC tracking maximizes the sparing of healthy tissue in the presence of respiratory motion during VMAT, while ensuring target coverage.

Declaration of Competing Interest

The authors declare that they have no known competing financial interests or personal relationships that could have appeared to influence the work reported in this paper.

Acknowledgements

The authors acknowledge funding by the Dutch Research Council (NWO) through project No. 17515 (BREATHE EASY). MLC tracking research at UMC Utrecht is performed under a research agreement with Elekta AB. We thank Peter Münger and Görgen Nilsson (ScandiDos) for providing research software for the Delta^4, and we thank Jochem Wolthaus for supporting the film dosimetry and Wilfred de Vries for assisting the Delta^4 measurements.

References

[1] Chang JY, Senan S, Paul MA, Mehran RJ, Louie AV, Balter P, et al. Stereotactic ablative radiotherapy versus lobectomy for operable stage I non-small-cell lung cancer: a pooled analysis of two randomised trials. Lancet Oncol 2015;16:630–7. https://doi.org/10.1016/S1470-2045(15)70168-3.

[2] Tekatli H, Haasbeek N, Dahele M, Haan PD, Verbakel W, Bongers E, et al. Outcomes of Hypofractionated High-Dose Radiotherapy in Poor-Risk Patients with " Ultracentral " Non – Small Cell Lung Cancer. J Thoracic Oncol 2016;11:1081–9. https://doi.org/10.1016/j.jtho.2016.03.008.

[3] Palma D, Visser O, Lagerwaard FJ, Belderbos J, Slotman BJ, Senan S. Impact of Introducing Stereotactic Lung Radiotherapy for Elderly Patients Impact of Introducing Stereotactic Lung Radiotherapy for Elderly Patients With Stage I Non – Small-Cell Lung Cancer: A Population-Based Time-Trend Analysis. J Clin Oncol 2010;28:5153–9. https://doi.org/10.1200/JCO.2010.30.0731.

[4] Fogliata A, Clivio A, Nicolini G, Vanetti E, Cozzi L. Intensity modulation with photons for benign intracranial tumours: A planning comparison of volumetric single arc, helical arc and fixed gantry techniques. Radiother Oncol 2008;89:254–62. https://doi.org/10.1016/j.radonc.2008.07.021.

[5] Holt A, Van Vliet-Vroegindeweij C, Mans A, Belderbos JS, Damen EM. Volumetric-modulated arc therapy for stereotactic body radiotherapy of lung tumors: A comparison with intensity-modulated radiotherapy techniques. Int J Radiat Oncol Biol Phys 2011;81:1560–7. https://doi.org/10.1016/j.ijrobp.2010.09.014.

[6] Kontaxis C, Woodhead P, Bol G, Lagendijk J, Raaymakers B. Proof-of-concept delivery of intensity modulated arc therapy on the Elekta Unity 1.5 T MR-linac. Phys Med Biol 2021;66:04LT07. https://doi.org/10.1088/1361-6560/abd66d.

[7] Rietzel E, Liu AK, Doppke KP, Wolfgang JA, Chen AB, Chen GT, et al. Design of 4D treatment planning target volumes. Int J Radiat Oncol Biol Phys 2006;66:287–95. https://doi.org/10.1016/j.ijrobp.2006.05.024.

[8] Klüter S. Technical design and concept of a 0.35 T MR-Linac, Clinical and Translational. Radiat Oncol 2019;18:98–101. https://doi.org/10.1016/j.ctro.2019.04.007.

[9] Ekberg L, Holmberg O, Wittgren L, Bjelkengren G, Landberg T. What margins should be added to the clinical target volume in radiotherapy treatment planning for lung cancer? Radiother Oncol 1998;48:71–7. https://doi.org/10.1016/S0167-8140(98)00046-2.

[10] Menten MJ, Fast MF, Nill S, Kamerling CP, McDonald F, Oelfke U. Lung stereotactic body radiotherapy with an MR-linac – Quantifying the impact of the magnetic field and real-time tumor tracking. Radiother Oncol 2016;119:461–6. https://doi.org/10.1016/j.radonc.2016.04.019.

[11] Seppenwoolde Y, Shirato H, Kitamura Kei, Shimizu S, Herk MV, Lebesque J, et al. Precise and Real-Time Measurement of 3D Tumor Motion in. Int J Radiat Oncol Biol Phys 2002;53(4):822–34. https://doi.org/10.1016/s0360-3016(02)02803-1.

[12] Song SY, Choi W, Shin SS, Lee SW, Ahn SD, Kim JH, et al. Fractionated stereotactic body radiation therapy for medically inoperable stage I lung cancer adjacent to central large bronchus. Lung Cancer 2009;66(1):89–93. https://doi.org/10.1016/j.lungcan.2008.12.016.

[13] Wolthaus JW, Sonke JJ, van Herk M, Belderbos JS, Rossi MM, Lebesque JV, et al. Comparison of Different Strategies to Use Four-Dimensional Computed Tomography in Treatment Planning for Lung Cancer Patients. Int J Radiat Oncol Biol Phys 2008;70:1229–38. https://doi.org/10.1016/j.ijrobp.2007.11.042.

[14] Finazzi T, van Sörnsen de Koste JR, Palacios MA, Spoelstra FO, Slotman BJ, Haasbeek CJ, et al. Delivery of magnetic resonance-guided single-fraction stereotactic lung radiotherapy. Phys Imag Radiat Oncol 2020;14:17–23. https://doi.org/10.1016/j.phro.2020.05.002.

[15] Parikh NR, Lee PP, Raman SS, Cao M, Lamb J, Tyran M, et al. Time-Driven Activity-Based Costing Comparison of CT-Guided Versus MR-Guided SBRT. JCO Oncol Practice 2020;16:e1378–85. https://doi.org/10.1200/jop.19.00605.

[16] Dhont J, Harden SV, Chee LY, Aitken K, Hanna GG, Bertholet J. Image-guided Radiotherapy to Manage Respiratory Motion: Lung and Liver. Clin Oncol 2020;32:792–804. https://doi.org/10.1016/j.clon.2020.09.008.

[17] Crijns SP, Raaymakers BW, Lagendijk JJ. Proof of concept of MRI-guided tracked radiation delivery: Tracking one-dimensional motion. Phys Med Biol 2012;57:7863–72. https://doi.org/10.1088/0031-9155/57/23/7863.

[18] Yun J, Wachowicz K, Mackenzie M, Rathee S, Robinson D, Fallone BG. First demonstration of intrafractional tumor-tracked irradiation using 2D phantom MR images on a prototype linac-MR. Med Phys 2013;40:051718. https://doi.org/10.1118/1.4802735.

[19] Fast MF, Nill S, Bedford JL, Oelfke U. Dynamic tumor tracking using the Elekta Agility MLC. Med Phys 2014;41:1–5. https://doi.org/10.1118/1.4899175.

[20] Keall PJ, Sawant A, Berbeco RI, Booth JT, Cho B, Cerviño LI, et al. AAPM Task Group 264: The safe clinical implementation of MLC tracking in radiotherapy. Med Phys 2021;48(5):e44–64. https://doi.org/10.1002/mp.14625.
[21] Booth J, Caillet V, Briggs A, Hardcastle N, Angelis G, Jayamanne D, et al. MLC tracking for lung SABR is feasible, efficient and delivers high-precision target dose and lower normal tissue dose. Radiother Oncol 2021;155:131–7. https://doi.org/10.1016/j.radonc.2020.10.036.
[22] Glitzner M, Woodhead PL, Borman PT, Lagendijk JJ, Raaymakers BW. Technical note: MLC-tracking performance on the Elekta unity MRI-linac. Phys Med Biol 2019;64:15NT02. https://doi.org/10.1088/1361-6560/ab2667.
[23] Liu PZ, Dong B, Nguyen DT, Ge Y, Hewson EA, Waddington DE, et al. First experimental investigation of simultaneously tracking two independently moving targets on an MRI-linac using real-time MRI and MLC tracking. Med Phys 2020;47:6440–9. https://doi.org/10.1002/mp.14536.
[24] Uijtewaal P, Borman PT, Woodhead PL, Hackett SL, Raaymakers BW, Fast MF. Dosimetric evaluation of MRI-guided multi-leaf collimator tracking and trailing for lung stereotactic body radiation therapy. Med Phys 2021;48:1520–32. https://doi.org/10.1002/mp.14772.
[25] Davies GA, Poludniowski G, Webb S. MLC tracking for Elekta VMAT: A modelling study. Phys Med Biol 2011;56:7541–54. https://doi.org/10.1088/0031-9155/56/23/013.
[26] Bedford JL, Fast MF, Nill S, McDonald FM, Ahmed M, Hansen VN, et al. Effect of MLC tracking latency on conformal volumetric modulated arc therapy (VMAT) plans in 4D stereotactic lung treatment. Radiother Oncol 2015;117:491–5. https://doi.org/10.1016/j.radonc.2015.07.044.
[27] Ferguson D, Harris T, Shi M, Jacobson M, Myronakis M, Lehmann M, et al. Automated MV markerless tumor tracking for VMAT Physics in Medicine & Biology. Phys Med Biol 2020;65:125011. https://doi.org/10.1088/1361-6560/ab8cd3.
[28] Booth JT, Caillet V, Hardcastle N, O'Brien R, Szymura K, Crasta C, et al. The first patient treatment of electromagnetic-guided real time adaptive radiotherapy using MLC tracking for lung SABR. Radiother Oncol 2016;121:19–25. https://doi.org/10.1016/j.radonc.2016.08.025.
[29] Shi X, Diwanji T, Mooney KE, Lin J, Feigenberg S, D'Souza WD, et al. Evaluation of template matching for tumor motion management with cine-MR images in lung cancer patients. Med Phys 2014;41:052304. https://doi.org/10.1118/1.4870978.
[30] Poulsen PR, Cho B, Sawant A, Ruan D, Keall PJ. Detailed analysis of latencies in image-based dynamic MLC tracking. Med Phys 2010;37:4998–5005. https://doi.org/10.1118/1.3480504.
[31] De Vries JH, Seravalli E, Houweling AC, Woodings SJ, Van Rooij R, Wolthaus JW, et al. Characterization of a prototype MR-compatible Delta4 QA system in a 1.5 tesla MR-linac. Phys Med Biol 2018;63:02NT02. https://doi.org/10.1088/1361-6560/aa9d26.
[32] Takao S, Miyamoto N, Matsuura T, Onimaru R, Katoh N, Inoue T, et al. Intrafractional baseline shift or drift of lung tumor motion during gated radiation therapy with a real-time tumor-tracking system a preliminary version of this study was presented at the 55th Annual Meeting of the American Society for Radiation Oncology. Int J Radiat Oncol Biol Phys 2016;94:172–80. https://doi.org/10.1016/j.ijrobp.2015.09.024.
[33] Lodeweges JE, van Rossum PS, Bartels MM, van Lindert AS, Pomp J, Peters M, et al. Ultra-central lung tumors: safety and efficacy of protracted stereotactic body radiotherapy. Acta Oncol 2021;60:1061–8. https://doi.org/10.1080/0284186X.2021.1942545.
[34] Keiper TD, Tai A, Chen X, Paulson E, Lathuilière F, Bériault S, et al. Feasibility of real-time motion tracking using cine MRI during MR-guided radiation therapy for abdominal targets. Med Phys 2020;47:3554–66. https://doi.org/10.1002/mp.14230.
[35] Tryggestad E, Flammang A, Hales R, Herman J, Lee J, McNutt T, et al. 4D tumor centroid tracking using orthogonal 2D dynamic MRI: Implications for radiotherapy planning. Med Phys 2013;40:091712. https://doi.org/10.1118/1.4818656.
[36] Seregni M, Paganelli C, Lee D, Greer PB, Baroni G, Keall PJ, et al. Motion prediction in MRI-guided radiotherapy based on interleaved orthogonal cine-MRI. Phys Med Biol 2016;61:872–87. https://doi.org/10.1088/0031-9155/61/2/872.